AGU PUBLICATIONS

JGR

Journal of Geophysical Research: Atmospheres

RESEARCH ARTICLE
10.1002/2015JD023107

Key Points:
- Precipitation signatures require care in their forward representation
- We have developed an approach to produce such a representation
- Our representation is very efficient and allows different possible microphysics

Correspondence to:
Z. S. Haddad,
zhaddad@jifresse.ucla.edu

Citation:
Haddad, Z. S., J. L. Steward, H.-C. Tseng, T. Vukicevic, S.-H. Chen, and S. Hristova-Veleva (2015), A data assimilation technique to account for the nonlinear dependence of scattering microwave observations of precipitation, *J. Geophys. Res. Atmos.*, *120*, 5548–5563, doi:10.1002/2015JD023107.

Received 12 JAN 2015
Accepted 1 MAY 2015
Accepted article online 10 MAY 2015
Published online 5 JUN 2015

A data assimilation technique to account for the nonlinear dependence of scattering microwave observations of precipitation

Z. S. Haddad[1,2], J. L. Steward[1,2], H.-C. Tseng[3], T. Vukicevic[4], S.-H. Chen[3], and S. Hristova-Veleva[1,2]

[1] Jet Propulsion Laboratory, California Institute of Technology, Pasadena, California, USA, [2] Joint Institute For Regional Earth System Science and Engineering, University of California, Los Angeles, California, USA, [3] Department of Land, Air and Water Resources, University of California, Davis, California, USA, [4] AOML, NOAA, Miami, Florida, USA

Abstract Satellite microwave observations of rain, whether from radar or passive radiometers, depend in a very crucial way on the vertical distribution of the condensed water mass and on the types and sizes of the hydrometeors in the volume resolved by the instrument. This crucial dependence is nonlinear, with different types and orders of nonlinearity that are due to differences in the absorption/emission and scattering signatures at the different instrument frequencies. Because it is not monotone as a function of the underlying condensed water mass, the nonlinearity requires great care in its representation in the observation operator, as the inevitable uncertainties in the numerous precipitation variables are not directly convertible into an additive white uncertainty in the forward calculated observations. In particular, when attempting to assimilate such data into a cloud-permitting model, special care needs to be applied to describe and quantify the expected uncertainty in the observations operator in order not to turn the implicit white additive uncertainty on the input values into complicated biases in the calculated radiances. One approach would be to calculate the means and covariances of the nonlinearly calculated radiances given an a priori joint distribution for the input variables. This would be a very resource-intensive proposal if performed in real time. We propose a representation of the observation operator based on performing this moment calculation off line, with a dimensionality reduction step to allow for the effective calculation of the observation operator and the associated covariance in real time during the assimilation. The approach is applicable to other remotely sensed observations that depend nonlinearly on model variables, including wind vector fields. The approach has been successfully applied to the case of tropical cyclones, where the organization of the system helps in identifying the dimensionality-reducing variables.

1. Introduction

The problem of assimilating such highly nonlinear observations as the microwave brightness temperatures measured over precipitating clouds by current satellite microwave instruments has been recognized as multifaceted, with specific attention required to (1) the estimation of the background hydrologic state of the atmosphere (the distribution of the condensed water mass into hydrometeors of varying habits, shapes, densities, and sizes), (2) the correlations between the variables, and (3) the imperfections in the representation of the dependence of the observations on the model variables [see, e.g., *Errico et al.*, 2007]. A few pioneering efforts [*Aonashi and Eito*, 2011; *Bauer et al.*, 2006; *Chen*, 2007; *Vukicevic et al.*, 2007; *Zhang et al.*, 2012] have addressed the first two problems. This paper summarizes our effort regarding the third problem, regarding the uncertainty in the dependence of these microwave observations on the underlying rain, especially to account for the complex nonlinearity of the forward radiation transfer relation between the variables and their signatures in the satellite measurements.

Suppose one has an atmospheric model which represents (and tracks the four-dimensional evolution of) the water mass, and one would like to assimilate satellite observations O that are most sensitive to the condensed water mass. Whether O consists of active signatures (such as a set of contiguous vertical profiles of radar reflectivity factors) or passive signatures (such as brightness temperatures measured at the top of a collection of contiguous radiometer beams), O can be represented as

$$O = F(\vec{x}, \vec{p}_b, \vec{p}_s) \; + \; \text{uncertainty} \tag{1}$$

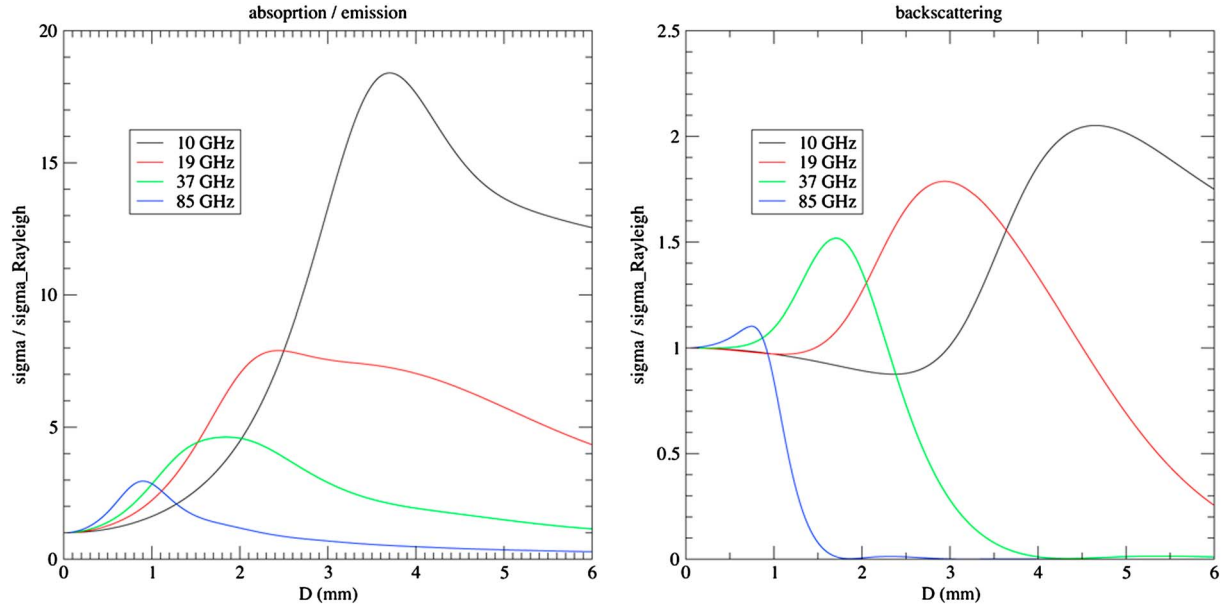

Figure 1. Plots of the Mie absorption and backscattering cross sections, normalized by the Rayleigh approximation (D^3 for the absorption and D^6 for the backscattering) for liquid spheres of diameter D.

where $\vec{x}$ consists of the model variables which affect O, $\vec{p}_b$ consists of the background model parameters which are neither prognostic nor diagnosed (such as the parameters controlling the shape of the assumed raindrop size distribution), and $\vec{p}_s$ consists of scattering parameters which the model does not represent at all but which the radiative transfer depends on (such as the parameters quantifying the shape of the hydrometeors).

In today's variational data assimilation approaches, the fundamental assumption that leads to the need to minimize a cost function featuring the difference $O - F$ is that F represents the mean of the remotely sensed signature associated to the variables $\vec{x}$. Indeed, the assimilation will start with a "background" value for $\vec{x}$ and proceed to adjust it based on how "close" the associated mean signature $F(\vec{x})$ comes to the measured O.

It is important to emphasize that F is meant to be the mean signature, because $\vec{x}$ itself is but a mean—the mean value of the model variables within the volume element resolved by the model. Indeed, this background value for $\vec{x}$ has to be accompanied by a covariance matrix B representing the second moment of the uncertainty in these mean background values, the first moment being 0 since the background is the a priori mean. The fundamental question is, given the mean $\vec{x}$ and its covariance B, how can we calculate the mean $F(\vec{x}, \vec{p}_b, \vec{p}_s)$? Why is a single forward calculation, where one inputs the values of the model variables in one's column $\vec{x}$ and the radiative transfer performs the forward calculation with just these exact input values, not sufficient?

The question has a practical aspect in the context of variational data assimilation, where the minimization of $O - F$ as in (1) may well require the evaluation of F repeatedly for different values of $\vec{x}$, and that process would need to be repeated for every observation. It is therefore not sufficient to provide a procedure to compute the mean of F, but rather one that can be efficiently implemented within the constraints of the typical assimilation exercise, where the results are required within a reasonable amount of time in order to produce an improved forecast, along with an improved analysis. Obtaining the mean F is very important regardless of the specific method that one plans to use for the assimilation, because the latter will convert the difference $O - F$ into adjustments to the model state variables, and this conversion will incur errors if $O - F$ has biases due to the nonlinearities of F.

2. The Case of Microwave Observations

If F were linear, the answer would be simple, as the mean of a function of a random variable is simply the function applied to the mean of the random variable. However, in our case, the radiative transfer function is not only highly nonlinear but it is not monotone in any one of the input components of $\vec{x}$ (let alone $\vec{p}_b$ or $\vec{p}_s$ [see, e.g., *Haddad et al.*, 2007]). Figure 1 illustrates the nonlinearity by plotting the absorption and

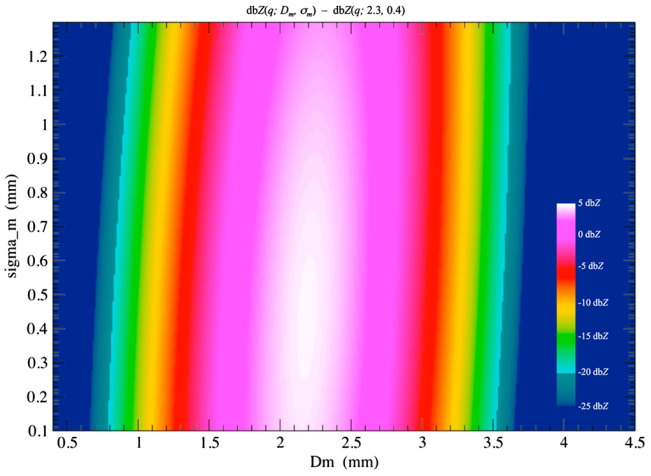

Figure 2. Values of the measured radar reflectivity factor at 35 GHz, or rather its deviation from the reference value obtained when the two parameters D_m = mass-weighted mean diameter and σ_m = mass-weighted diameter standard deviation are assumed to have midrange values of 2.3 mm and 0.4 mm, respectively.

backscattering cross sections as a function of diameter for liquid spheres at different frequencies. Not only do the best power law approximations start to fail for small drop sizes, at all frequencies, but the coefficients of the approximate power laws increase with the smallest sizes then reach a maximum and decrease for the larger drop sizes. The cumulative effect on the measured signature is difficult to illustrate for the passive measurements since they are integrated over a variable vertical distribution of condensed water mass, but it can be appreciated more readily in the case of the active measurement of a radar since the latter is directly sensitive to a specific height (within the range resolution of one's instrument, which is a few hundred meters for today's spaceborne radars). This is illustrated in Figure 2, plotting the radar reflectivity factor $F(x, p_1, p_2)$ as a function of the two parameters p_1 = mean drop diameter (on the horizontal axis) and p_2 = drop diameter standard deviation (on the vertical axis) in dB and after dividing by $F(x, 2.3, 0.4)$ to remove the dependence on the mixing ratio x (under the assumption that the probability distribution of the drop sizes is gamma and therefore depends on only two parameters). Instead of being linear or even monotone in p_1, the function clearly has a maximum near $(p_1 = 2.2, p_2 = 0.44)$ with a rapid falloff that precludes any linear approximation from being valid over much of a neighborhood about any a priori midrange parameter values such as (2.3 and 0.4).

Figures 1 and 2 illustrate the nonlinearity of F as a function of the two size parameters. The nonlinearity in the condensed water mixing ratios themselves is more complicated still, as the measured signatures are the result of the competing effects of emission and out-of-beam scattering in the passive case, and backscattering and attenuation in the active case. Figure 3 illustrates the total resulting effect on the brightness temperatures that would be measured over a simulated tropical cyclone, in this case an Hurricane Weather Research and Forecasting (HWRF) [see *Gopalakrishnan et al.*, 2013, and the references therein] forecast of Hurricane Earl on 31 August 2010. The figure shows the spatial variability of the brightness temperatures that would be observed over the hurricane at the frequency/polarization combinations of the Tropical Rainfall Measuring Mission (TRMM) Microwave Imager (TMI) [see *Kummerow et al.*, 1998]. The 10.7 GHz channels delineate the area of rain, with higher temperatures due mostly to emission from the liquid rain drops, while the 85.5 GHz channels show the locus of the snow and graupel, with cooler temperatures due mostly to out-of-column scattering of the upwelling radiation by the solid hydrometeors.

Figure 4 shows the results of the forward calculations with the same values as Figure 3 except for the rain and graupel whose mean diameter is now assumed smaller by 44% and except for the graupel density which is now assumed to be half of its value in the calculation of Figure 3. In addition to the general reduction in the warming observed in the 10.7 GHz channels and the large reduction in the cooling observed in the 85.5 GHz channels, note the more subtle changes in the 19.3 and 21.3 GHz channels, where the competing effects of emission and scattering lead to a different reduction or enhancement of the signature as one moves from the outer edge of the rain band toward the center of the vortex. In order for one's forward observation operator to reflect these mutually ambiguous differences, one would need to repeat the forward radiative transfer

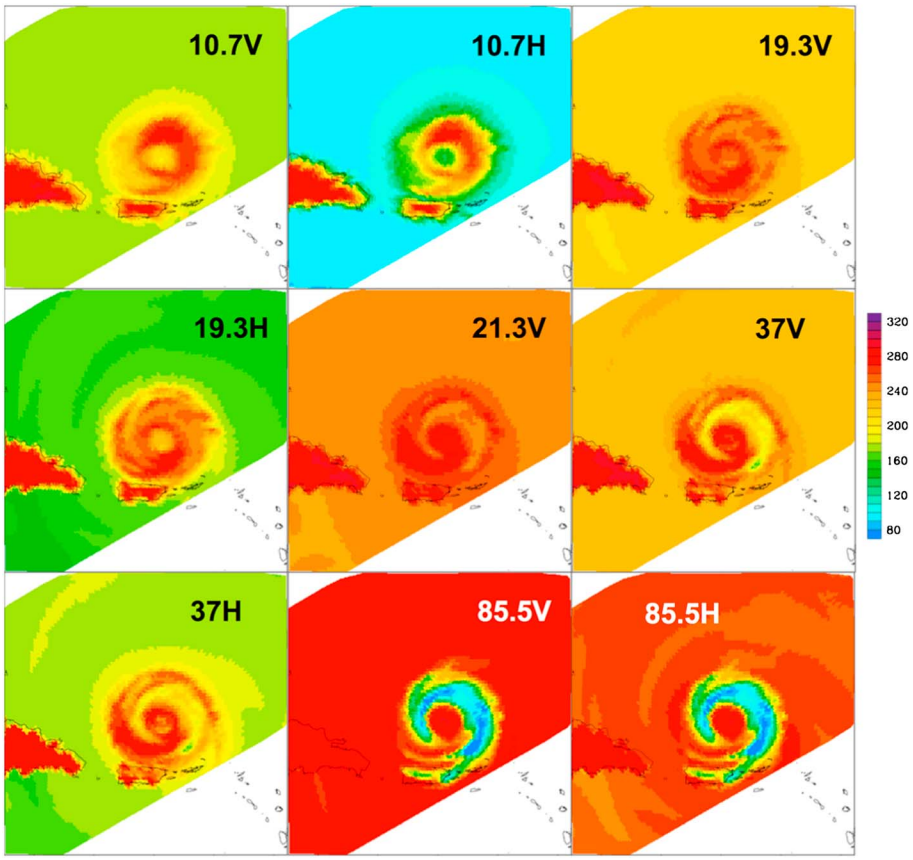

Figure 3. Brightness temperatures for an HWRF simulation of Hurricane Earl on 31 August 2010 at 0600 Z, calculated using Community Radiative Transfer Model (CRTM) with the default microphysical parameter values.

calculation for a very large number of perturbations of the input variables and parameters, a proposition that is simply not feasible in the context of data assimilation where performing repeated forward calculations for each observation over each grid point at each iteration of the analysis is prohibitively resource intensive.

3. Empirical Dimensionality Reduction

If one had vast amounts of computational resources (and time), one could contemplate calculating $F(\vec{x}, \vec{p}_b, \vec{p}_s)$ by starting with the mean value for $\vec{x}$ that one has as input, along with the putative "mean" values of the parameters that are used by the dynamical model and the forward radiative transfer function and then repeat the calculation by varying these values one at a time according to the a priori uncertainty estimates that one has. There are three problems with this approach:

1. The approach requires knowledge of the uncertainty in the parameters, and the latter is not readily available. For example, the typical microphysical schemes make the assumption that the raindrop diameters have an exponential distribution, with the so-called "number concentration intercept" N_T/D fixed a priori (N_T being the total number of drops per unit volume, and D being the mean diameter)—and the single coefficient in the exponent of the exponential distribution is then set to produce the required mixing ratio. The parameter N_T/D is fixed a priori for the entire domain over the entire duration of the model run, yet a very large variability (several orders of magnitude) for this parameter is observed from in situ samples of raindrop size distributions. Moreover, little is known about the spatial or temporal behaviors of this parameter.
2. The approach requires knowledge of the joint behavior of the parameters and the variables. Indeed, it is not sufficient to have a standard deviation on N_T/D, to take this parameter as an example. One still needs to know its correlation with the mixing ratios themselves.
3. The approach would be prohibitively expensive. The expense of performing repeated forward radiative transfer calculations is most significant if one had to perform them in real time.

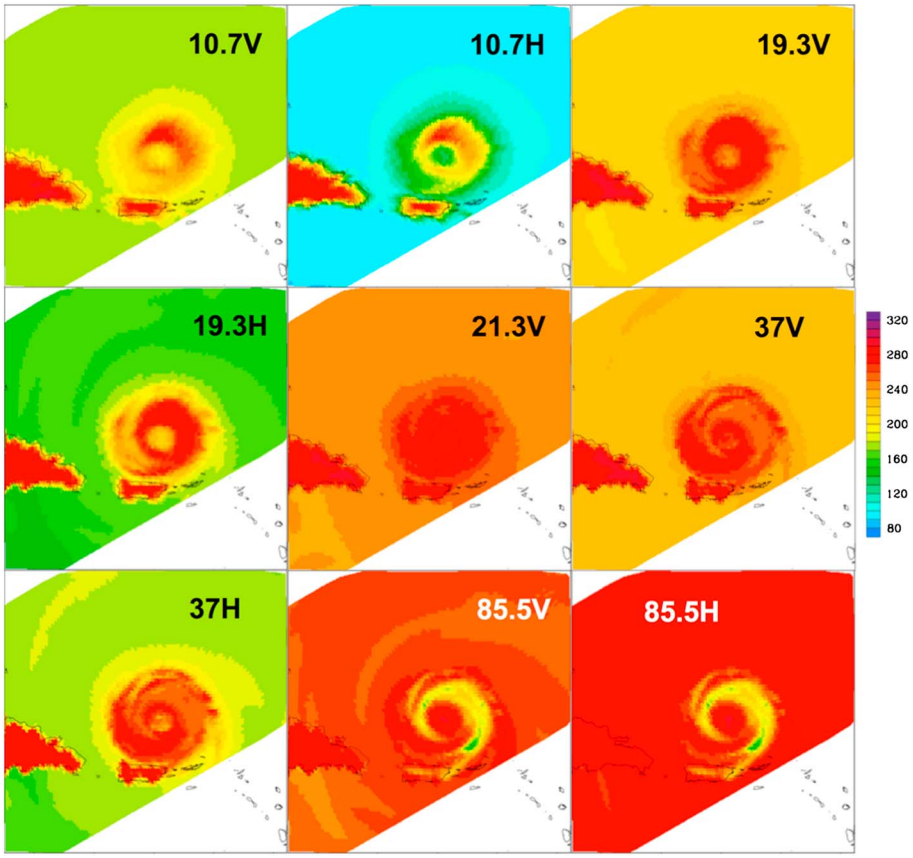

Figure 4. Brightness temperatures over the HWRF simulation of Hurricane Earl as in Figure 3, calculated using CRTM with adjusted microphysical parameter values (raindrops smaller by 44%, smaller graupel that is half as dense as Figure 3).

Of the three objections, the third may well be the easiest to circumvent. If the forward calculation of the brightness temperatures could be performed ahead of time, off line, and stored in a large database, one could conceive of a modified approach where the database would be searched in real time to estimate the required signatures from the precomputed stored values. Mathematically, in real time one would compute

$$F(\vec{x},\vec{p}_b,\vec{p}_s) \;=\; C^{-1} \sum_{\vec{x}^{(k)}\in \text{database}} O^{(k)} \exp\left(-0.5||\vec{x}-\vec{x}^{(k)}||^2\right) \tag{2}$$

where each $\vec{x}^{(k)}$ is a sample input (from the database), $O^{(k)}$ is the corresponding output of the exact radiative transfer calculation with input $\vec{x}^{(k)}$, and $||...||^2$ is a norm that quantifies the distance between one's real-time input and the different members of the database (and C is a normalization constant consisting of the sum on the right without "$O^{(k)}$"). The database can be constructed from a collection of columns above model grid points taken from different times of different model simulations of precipitating systems. To the variable values $\vec{x}^{(k)}$ in each column, one associates the exact forward calculated microwave signatures $O^{(k)}$ that one is interested in. One can repeat the process with different values of the dynamical and radiative transfer parameters and thereby assemble a very large database that would represent the variability of the variables and parameters for one's physical regime and use (2) in real time to estimate the mean observation corresponding to a mean input $\vec{x}$.

What makes (2) completely impractical is the large dimension of $\vec{x} \in \mathbb{R}^N$: the vector has to include the temperatures and mixing ratios at each level of a layered atmosphere, so counting at least one mixing ratio for each of the three phases of water for each of the 30 or so layers in our vertically stratified atmosphere, along with the temperature, N must be at least 120—and the distance in the exponent of (2) would need to be computed in this very large dimensional space. Our proposal *to reduce the dimensionality is to apply a simultaneous change of coordinates to the variables as well as the observations.* If we arrange the simultaneous observations

over a given grid point, say M of them (and $M = 9$ in the case of TMI, as in Figures 3 and 4; in the case of a vertically profiling radar, M would be the number of vertical levels at which the radar measured the reflectivity factor) into a vector $\vec{O} = (O_1, ..., O_M)$, we seek to determine the pair of vectors $\vec{a} \in \mathbb{R}^M$ and $\vec{b} \in \mathbb{R}^N$ such that $\vec{a}^t\vec{O}$ and $\vec{b}^t\vec{x}$ are maximally correlated. Mathematically, we are looking for $\vec{a}$ and $\vec{b}$ which maximize the square of the correlation coefficient

$$\frac{\mathcal{E}\left\{\left(\vec{a}^t \cdot (\vec{O} - \mathcal{E}\{\vec{O}\})\right) \cdot \left(\vec{b}^t \cdot (\vec{x} - \mathcal{E}\{\vec{x}\})\right)\right\}^2}{\mathcal{E}\left\{\left(\vec{a}^t \cdot (\vec{O} - \mathcal{E}\{\vec{O}\})\right)^2\right\} \cdot \mathcal{E}\left\{\left(\vec{b}^t \cdot (\vec{x} - \mathcal{E}\{\vec{x}\})\right)^2\right\}} \tag{3}$$

in which the notation "$\mathcal{E}\{...\}$" denotes the expected value of whatever is inside the braces. The function (3) is the ratio of two simple quartic polynomials in the coefficients of $\vec{a}$ and $\vec{b}$, and its extrema are not difficult to determine. In fact, if we use the covariance matrices $C_{O,x}$ (of $\vec{O}$ and $\vec{x}$), C_O (of $\vec{O}$ with itself), and C_x (of $\vec{x}$ with itself), which can be estimated from the database directly, one can show (as did *Hotelling* [1936]) that the expression (3) is maximized exactly when $\vec{a}$ and $\vec{b}$ satisfy

$$C_O^{-1} C_{O,x} C_x^{-1} C_{O,x}^t \cdot \vec{a} = \lambda \vec{a} \tag{4}$$

$$C_x^{-1} C_{O,x}^t C_O^{-1} C_{O,x} \cdot \vec{b} = \lambda \vec{b} \tag{5}$$

for some scalar λ. These two equations convey a large amount of information and deserve a detailed discussion. They say that the matrices $C_O^{-1} C_{O,x} C_x^{-1} C_{O,x}^t$ (a relatively small $M \times M$ matrix) and $C_x^{-1} C_{O,x}^t C_O^{-1} C_{O,x}$ (a relatively large $N \times N$ matrix, with a lower rank equal to M) have the same non-0 eigenvalues, call them λ_1, ..., λ_M, and each eigenvector pair $(\vec{a}_i, \vec{b}_i)$ associated to a given eigenvalue λ_i corresponds to a local maximum in the correlation function (3). Equations (4) and (5) thus produce a hierarchy of M linear combinations of variables $\vec{b}_1^t\vec{x}$, ..., $\vec{b}_M^t\vec{x}$, each of which locally maximizes the correlation with a corresponding linearly transformed observation $\vec{a}_1^t\vec{O}$, ... , $\vec{a}_M^t\vec{O}$.

Rather than applying this dimensionality reduction procedure directly to the variables as they are represented by the model and the observations as they are produced by the instrument, we apply a preliminary "noise-filtering" step to extract the essential information content of these quantities. This preliminary step consists in a principal component analysis which we shall now describe. On the observation side, we know that the individual scalar measurements O_i constituting $\vec{O}$ are mutually correlated. For example, correlation analyses of the nine brightness temperatures (in Kelvin) measured simultaneously over any given location by TMI have principal components whose variances are on the order of

$$6000 \; > \; 1000 \; > \; 300 \; > \; 70 \; > \; 30 \; > \; 6 \; > \; 4 \; > \; 0.2 \; > \; 0.1 \tag{6}$$

[see, e.g., *Coppens et al.*, 2000]. Given that the RMS amplitude of the noise in the measured brightness temperatures is at least 2 K, the measurements cannot be relied upon to estimate the last two principal components. That is why in this case, in our dimensionality-reducing procedure, instead of $\vec{O} = (O_1, ..., O_9)$, we would start with the vector consisting of the top seven brightness temperature principal components $(O'_1, ..., O'_7)$. Similarly, for the model variables, we start by normalizing the temperatures by the single scalar global temperature standard deviation, and the mixing ratio of each water species by the single scalar global standard deviation of that mixing ratio, before performing a principal component analysis on the vector random variable consisting of the normalized model variables over a single model grid point. The specific number n ($< N$) of components $(x'_1, ..., x'_n)$ to retain will depend on the estimate of the uncertainties in the model variables, which themselves depend on the model, the original background covariances, and what information may have already been assimilated—in general, if the relative RMS uncertainty on any one variable is no better than r%, one would not want to retain the model principal components whose eigenvalue is smaller than r^2, because the values produced by the model are already noisier than that principal component's overall variance.

Once these two principal component analyses (on the observations and the prognostic variables) have been performed, it is the top principal components $(x'_1, ..., x'_n)$ and $(O'_1, ..., O'_m)$ that are used in the dimensionality reduction step (4) + (5), with $n < N$ and $m < M$, to obtain

$$\vec{a}_i^t\vec{O}' \; = \; F_i(\vec{x}, \vec{p}_b, \vec{p}_s) \; = \; C^{-1} \sum_{\vec{x}^{(k)} \in \text{database}} \vec{a}_i^t O'^{(k)} \exp\left(-0.5 \sum_{j=1}^{m} \left[\vec{b}_j^t\vec{x}' - \vec{b}_j^t\vec{x}'^{(k)}\right]^2\right) \tag{7}$$

Expression (7) effectively estimates the conditional mean of each scalar $\vec{a}_i^t \vec{O}'$ (for $i = 1, ..., m$), conditioned on $\vec{x}$. The obvious linear transformation then produces $O'_1, ..., O'_m$, and if one uses these with the overall mean for the lowest principal components $O'_{m+1}, ..., O'_M$, one can effectively reconstruct the mean of the full observation $\vec{O}$ that would be associated with $\vec{x}$. Note that the sample covariances can be obtained from the same database, using the corresponding formula. This is the basic approach that is illustrated in the next section.

Equation (7) provides a representation of the observation operator that is unbiased relative to the uncertainties in $\vec{x}, \vec{p}_b, and \vec{p}_s$ and that can be implemented very efficiently in practice. However, to complete a variational data assimilation, one still needs to minimize one's cost function expressing the departure of the analyzed variables from their background values along with the departure of the forward calculated observations from the actual measurements. For highly nonlinear functions F such as those we are considering, the tangent linear approximation to F can be used to find the minimum. When using (7) for F, the tangent linear approximation is very simple to use explicitly—indeed, the dependence of F on each variable is made completely explicit in the exponent of (7), and all the partial derivatives can be explicitly calculated directly from (7). In other words, the main impact of our approach is not on the minimization procedure itself: rather, it is on how to effectively calculate the mean value of F (around which the tangent linear approximation will be valid, in the minimization step), instead of using the single forward calculation option, which does not begin to capture the effects of the uncertainty in $\vec{x}$ or, equally importantly, in the background model parameters $\vec{p}_b$ and the radiative transfer-specific parameters $\vec{p}_s$. In brief, our representation (7) of F can be used with *all* existing assimilation approaches—what it adds is to allow a more accurate and more efficient evaluation of the mean F (and of its derivatives, if required) that accounts for the biases resulting from the nonlinear dependence on input uncertainty.

4. First Tests

Since this approach is specifically to deal with the representation of the microwave observation operator as a function of the prognostic variables of one's cloud model, while accounting for the fixed parameters, it is important to illustrate the range of variability of these quantities and the different options to account for them in the representation of the observation. We performed our first tests on Weather Research and Forecasting (WRF) [*Michalakes et al.*, 2001] simulations of Hurricane Rita from 0000 Z on 21 September 2005 to 1200 Z on 22 September 2005, with three nested grids having horizontal resolutions of 12, 4, and 1.33 km. The first simulation used the Thompson microphysical scheme with a single-moment representation of the rain [*Thompson et al.*, 2008]. One of the first issues that required investigation is the normalization of the different variables, in order for the approach not to misinterpret the different units of different quantities as temperature and mixing ratio. Before delving into the specific results, we start with a brief run-through of our approach as it proceeds in this specific case. We first collect all the output vectors over every grid point in the simulation:

$$\left(\chi_1, ..., \chi_{30}, \psi_1, ..., q_{pl,12}, ..., q_{g,30}\ ;\ T_{b,1}, ..., T_{b,9}\right)|_{(x_1,y_1),t=t_1}$$

$$\left(\chi_1, ..., \chi_{30}, \psi_1, ..., q_{pl,12}, ..., q_{g,30}\ ;\ T_{b,1}, ..., T_{b,9}\right)|_{(x_2,y_2),t=t_1}$$

$$\cdots$$

$$\cdots$$

$$\cdots$$

$$\left(\chi_1, ..., \chi_{30}, \psi_1, ..., q_{pl,12}, ..., q_{g,30}\ ;\ T_{b,1}, ..., T_{b,9}\right)|_{(x_K,y_K),t=t_L}$$

where χ_1 is the value of the potential at vertical level 1, ... , χ_{30} the potential at level 30, ψ is the stream function, ..., q_{pl} the precipitating liquid mixing ratio, ..., q_g the graupel mixing ratio; all taken at all the model's vertical layers over a fixed grid point at a fixed time output of the simulation, and we collect together all these column vectors over all grid points $(x_1, y_1), ..., (x_K, y_K)$ possibly at different instantaneous times $t_1, ..., t_L$—this collection

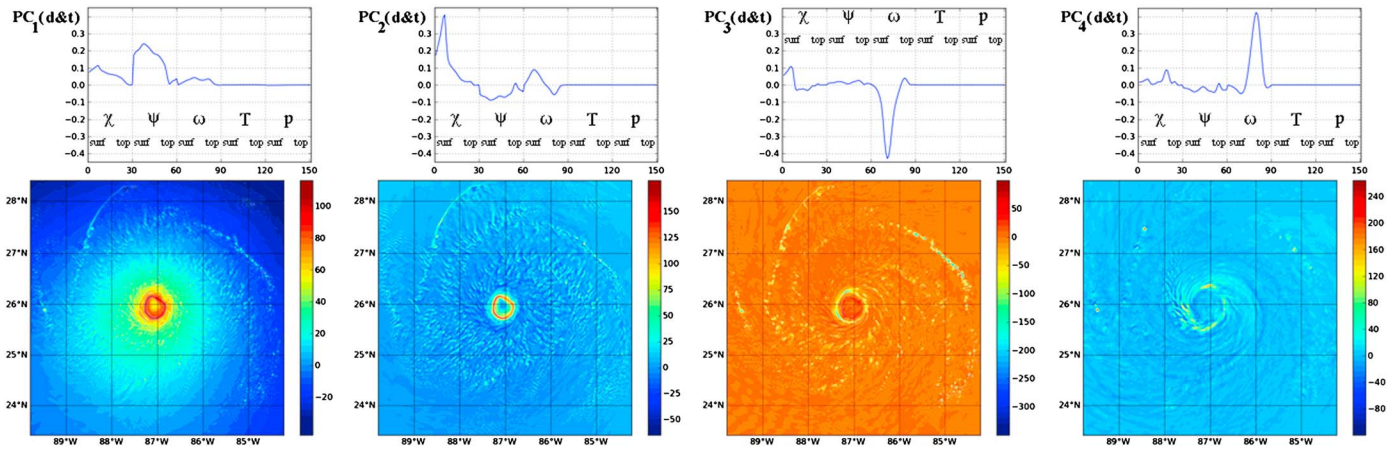

Figure 5. (top row) Coefficients of the first four vertical principal components of the dynamical and thermodynamical variables (velocity potential in each of the 30 layers numbered from the surface, followed by the 30 stream function variables, the 30 vertical velocity variables, the 30 temperatures, and the 30 pressures) calculated from the output of our WRF simulation of Hurricane Rita at 1800 Z on 21 September 2005. In this analysis, all the temperatures were normalized by the single global temperature standard deviation, as were the pressures, the vertical velocities, the stream functions, and the velocity potentials. The simulation used the Thompson microphysical scheme. (bottom row) The values of each of the four principal components over the two-dimensional grid.

is meant to represent the variety of value combinations that the model produces subject to the microphysical assumptions that we make (and one can stick to outputs from a single simulation with a single microphysical scheme or throw together outputs from simulations that allow different schemes or different parameter values in the same scheme, to represent the variability that one would like to account for). For each column vector, we also forward calculate the brightness temperatures corresponding to the inputs in each vector—in this case, these are the nine TMI brightness temperatures T_1, ..., T_9 at the bottom of each vector. Each vector thus represents one possible state of a vertical column of atmosphere along with its corresponding microwave signatures, and we collect these in a very large database consisting of thousands of such columns. To define the vectors $\vec{O}'$ and $\vec{x}'$ as in (7), we calculate the sample covariances of $(T_1, ..., T_9)$ to produce the 9×9 matrix C_O as in equations (4) and (5) and similarly the sample covariance matrix C_x for the model variables, from this same data set. Diagonalizing C_O and C_x allows us to define the new derived variables $\vec{x}'$ and the new derived observations $\vec{O}'$, which we then correlate with one another by finding the coefficients $\vec{a}_1$ of the linear combination of the entries of $\vec{O}'$ and the coefficients $\vec{b}_1$ of the linear combination of the entries of $\vec{x}'$ which are most correlated to one another—this pair is the first solution pair to the coupled eigenvalue problem (4) + (5). This final step, of identifying the coefficients $\vec{a}_i$ of the brightness temperature principal components which best correlation with a corresponding combination (with coefficients $\vec{b}_i$) of the model-variable principal components, can be repeated for each of the nine eigenvalues of the 9×9 matrix $C_O^{-1} C_{O,x} C_x^{-1} C_{O,x}^t$ to obtain nine pairs of coefficient vectors $(\vec{a}_i, \vec{b}_i)$, $i = 1, ..., 9$.

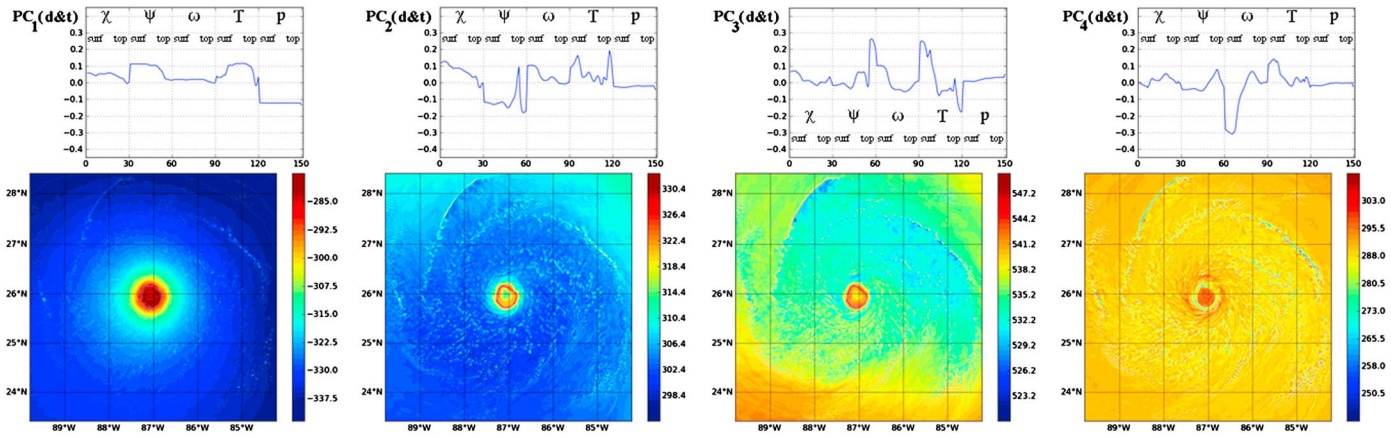

Figure 6. Same as Figure 5 with the exception that in this analysis each variable was normalized by the pressure-level-specific standard deviation.

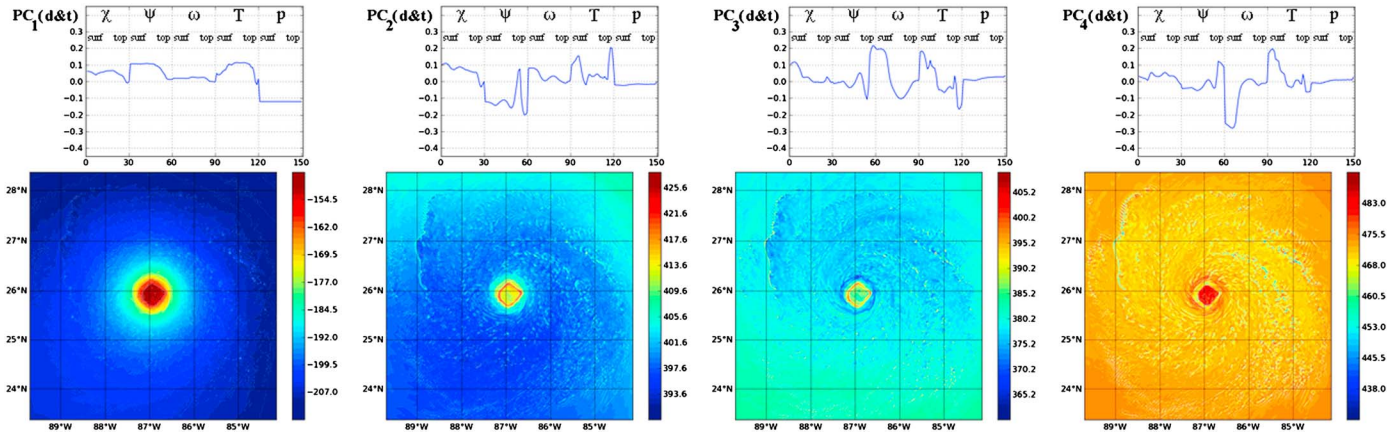

Figure 7. Same as Figure 5 with the exception that this simulation used the WSM6 microphysical scheme.

Figure 5 illustrates the results of the first step of the approach, the principal component (PC) analysis of the vertical vector of control (thermo)dynamical variables, in the case where the overall standard deviation of each species is used as the normalizing constant, and Figure 6 contrasts this with the same analysis using height-specific standard deviations instead (so one normalizing scalar per variable per pressure level, instead of one normalizing scalar per variable overall). Note how the first PC (ordered according to decreasing variance) in the former case is essentially the average of the stream function, the second is the near-surface velocity potential, the third is the midlevel vertical velocity, and the fourth is the upper level vertical velocity, whereas the PCs in the latter case are very different, starting with a first PC that still uses the average of the stream function along with the temperature minus the pressure. We confined the analysis to the control variables that do not describe the water contents specifically to evaluate the effect of the latter on the former. There is a definite sensitivity, and while the resulting representation (7) is not systematically different in the two cases, the derivatives appear to be. This is to be expected since the specific change of variable implied in (7) is different in the two cases, but the effect needs to be quantified and analyzed further. All the assimilation tests that we performed were using an ensemble Kalman-Filter approach that does not require derivatives, so this analysis is yet to be conducted.

We next tested the sensitivity to different microphysical assumptions, by performing the same principal component analysis of the (thermo)dynamical variables only, for the output of a simulation of Rita with the same WRF setup, where we used the WSM6 microphysical scheme [*Hong and Lim*, 2006] instead of Thompson. The The first two principal components (shown in Figure 7) confirm that the hurricane generated using WSM6 does appear similar to the one generated with Thompson, but the detailed analysis reveals substantial differences already in the third principal component, which has a more significant dependence on the vertical

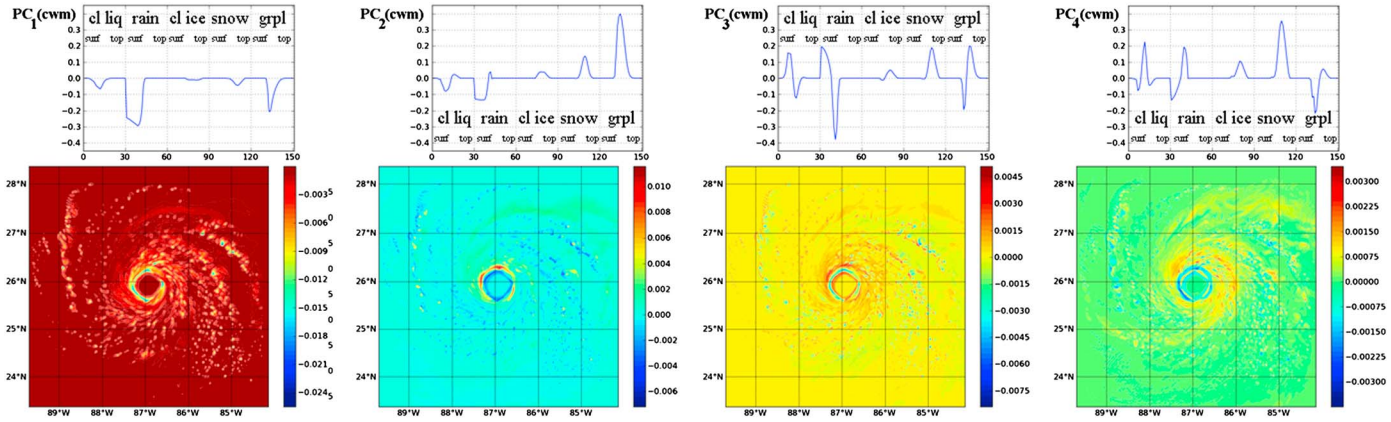

Figure 8. Same as Figure 7 with the exception that the variables here are the 30 cloud-liquid mixing ratios, followed by the precipitating liquid mixing ratios, the cloud-ice mixing ratios, the snow mixing ratios, and the graupel mixing ratios.

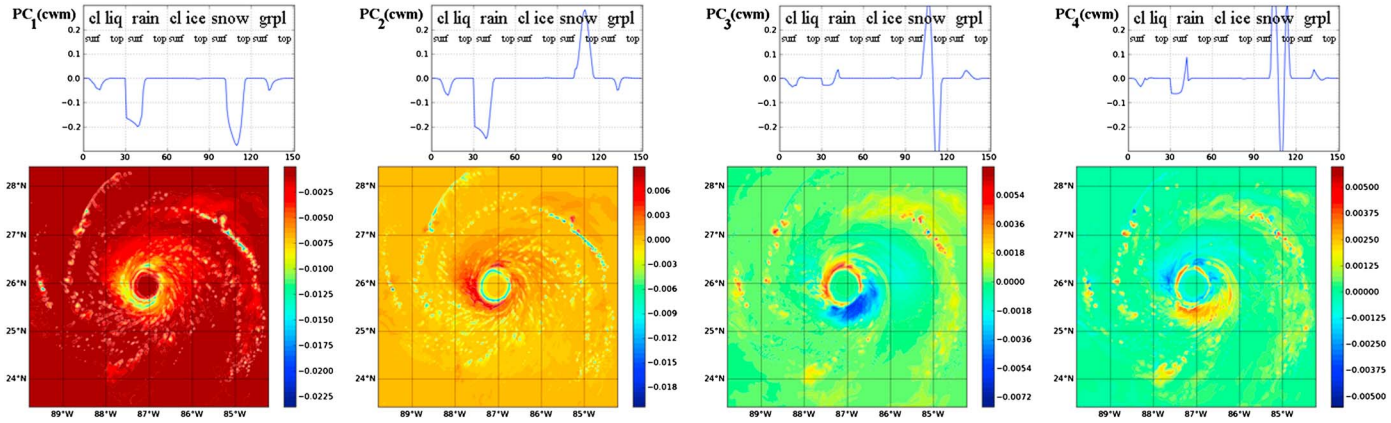

Figure 9. Same as Figure 8 except that this analysis is for the simulation using the Thompson microphysical scheme.

velocity in the WMS6 case, manifesting itself with a greater fine-scale variability at the different updrafts and downdrafts in the storm. Figures 8 and 9 show further differences in the vertical principal components of the water mixing ratios, as expected, starting at the third principal component (the second is different in the amplitude of the relative contributions of snow and graupel). In practice, one may typically wish to include in one's database columns from simulations using the same microphysical scheme as will be used in the dynamical model, allowing for the parameter perturbations that are realistic for one's case. However, if one does not wish to emphasize a single scheme, for example, in the case of a 1-D Var approach (such as the one developed by *Boukabara et al.* [2011]) that would start with an archival background in order for the assimilation to produce, in effect, a retrieval (without enforcing a single set of simplifying microphysical assumptions), then including simulations with different microphysical schemes in one's database would be very much desirable, and the approach we are proposing is the only approach to date that allows one to write down a representation of the observation operator that accounts for the uncertainty due to different possible microphysical assumptions.

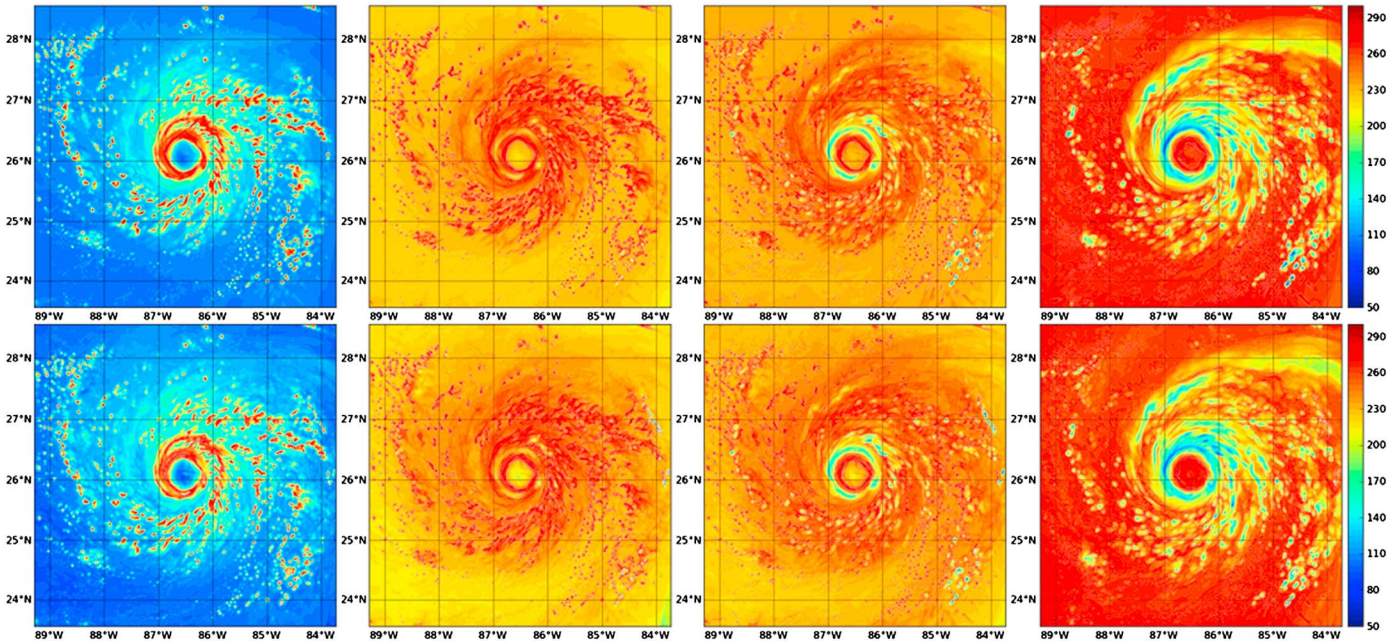

Figure 10. (top row) Brightness temperatures at the 10.7 GHz-Hpol, 19.3 GHz-Vpol, 37 GHz-Vpol, and 85.5 GHz-Vpol channels of TMI, calculated using SOI from the output of our WRF simulation (with WSM6 microphysics) of Hurricane Rita at 0000 Z on 22 September 2005. (bottom row) brightness temperatures in the same TMI channels calculated using our approach (7) from the database consisting of the output of our simulation at 1200 Z on 22 September with all nine TMI channels calculated by SOI (to build the database). In our approach (7), we retained only the top $m = 3$ maximum-correlation vectors and used the sample means of the other six from the database (of the 1200 Z output).

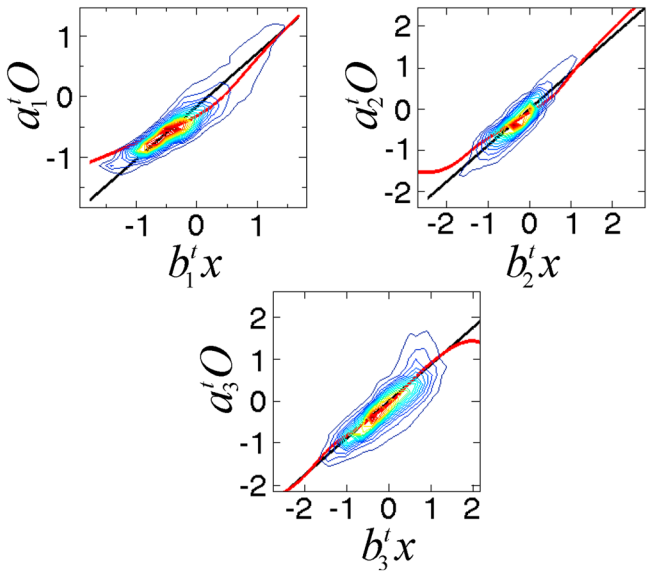

Figure 11. Joint distribution of the first three pairs ($a_i^t \vec{O}'$, $b_i^t \vec{x}'$) derived from the top-of-the-hour output of HWRF simulations of Hurricane Earl from 29 August to 2 September 2010, evaluated at the half-hour outputs. The black line is the linear regression of the transformed observation in terms of the transformed variables, and the red line is the conditional mean of the former given the latter. The contour lines are five percentage points apart ("vigintiles").

We next verified the ability of the resulting operator (7) to reproduce the expected brightness temperature ranges that one obtains from the single forward radiative transfer calculations. Figure 10 illustrates this on the same case of Hurricane Rita, for the four TMI channels where the advantages and disadvantages appear most clearly. Figure 10 (top row) shows the exact brightness temperatures calculated at the 10.7 H, 19.3 V, 37 V, and 85.5 V frequency-polarization combinations by the successive order of interaction (SOI) radiative transfer model [*Heidinger et al.*, 2006] from our Rita simulation output at 0000 Z on 22 September. Figure 10 (bottom row) shows the brightness temperatures calculated by our representation, using a database compiled out of the SOI-calculated brightness temperatures corresponding to the model values at 1200 Z on 22 September (when the simulated storm center was near 88.2 W, 26.8 N). Three features deserve special mention: the general emission signature at the lowest frequency (essentially, increasing emission as the condensed water mass increases) is quite well reproduced; similarly, the scattering signature at the highest frequency (mainly cooling from increasing scattering as the condensed water mass increases) is well reproduced, though the absorption by lighter and shallower condensation is less consistently represented, most evident in the northwest corner north of 27°N and west of 88°W; and the conflict between emission and scattering at the middle frequencies does produce some differences, most visible in the nearly linear northwest-to-southeast streak

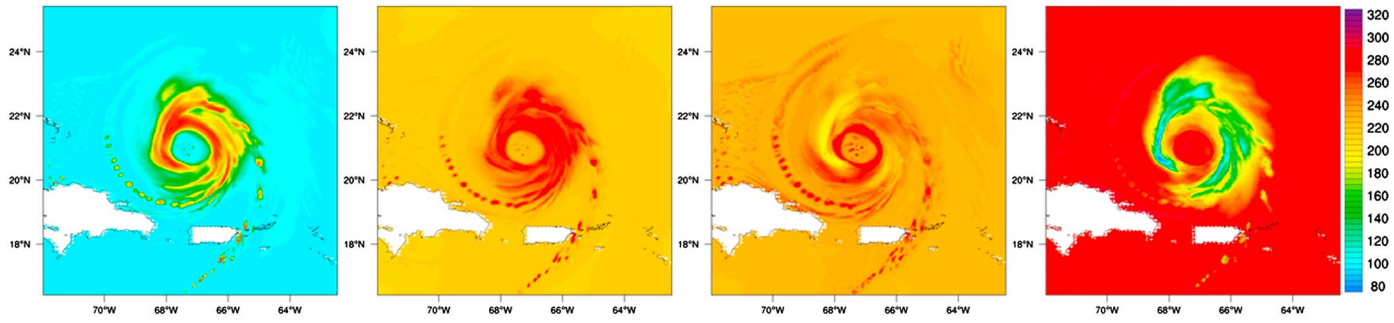

Figure 12. Brightness temperatures at the 10.7 GHz-Hpol, 19.3 GHz-Vpol, 37 GHz-Vpol, and 85.5 GHz-Vpol channels of TMI, calculated using our approach (equation (7) retaining only the top $m = 3$ maximum-correlation vectors) from the output of our HWRF simulation of Hurricane Earl at 0430 Z on 31 August 2010. The database consisted of the output of HWRF at the half hour from 29 August to 3 September.

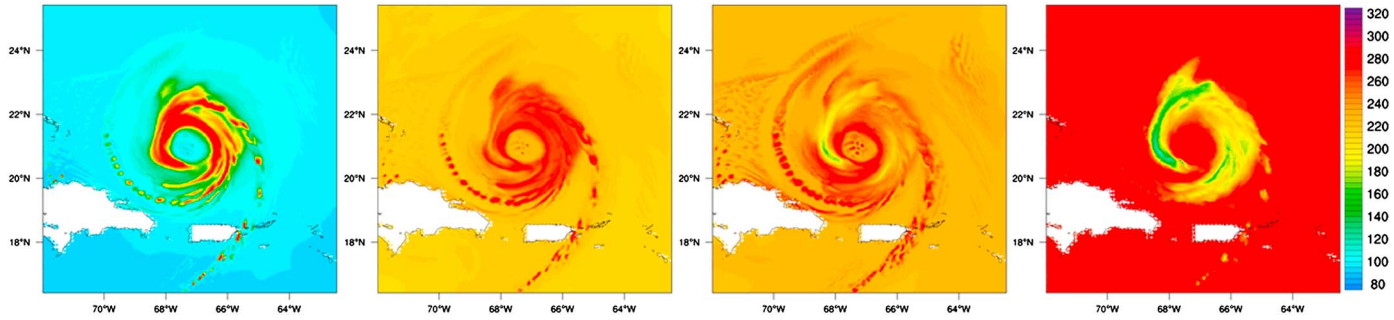

Figure 13. Brightness temperatures at the 10.7 GHz-Hpol, 19.3 GHz-Vpol, 37 GHz-Vpol, and 85.5 GHz-Vpol channels of TMI, calculated using CRTM from the output of our HWRF simulation of Hurricane Earl at 0430 Z on 31 August 2010 (as in Figure 12).

centered at 84°W × 27°N. Keep in mind that our representation is not meant to coincide with any single forward calculation, but rather, the mean of the brightness temperatures for one's atmospheric state.

Our first ensemble data assimilation test was with the HWRF Ensemble Data Assimilation System [*Aksoy et al.*, 2012]. The database that we used was built out of top-of-the-hour output of HWRF simulations of Hurricane Earl from 29 August to 2 September 2010. The TMI brightness temperatures corresponding to each column of atmospheric variables were calculated using CRTM [*Han et al.*, 2006] and RTTOV [*Matricardi et al.*, 2001], resulting in two entries in the database per forecast column. Figure 11 shows the joint distribution of the results of our dimensionality reduction ((4) and (5)) on this simulated data, for the top three maximal-correlation combination pairs. Figure 12 illustrates the resulting brightness temperatures out of our approach (7) when the input values were from one member of the Hurricane Ensemble Data Assimilation System (HEDAS) ensemble at 0430 Z. These values can be compared with the single forward calculation using CRTM (Figure 13) or RTTOV (Figure 14). The comparison reveals that over the precipitation, CRTM is warmer than RTTOV at the lowest frequency and at the highest frequency—and our approach produces values between the two, as expected. At 19.3 and 37 GHz, different regions appear warmer or cooler with CRTM than with RTTOV depending on the interplay between the scattering and the emission, yet the results of our approach are not consistently between the two—indeed, in a narrow ring-like region at the center of the eyewall, our operator produces 19.3 GHz brightness temperatures that are up to 5 K warmer than those of either CRTM or RTTOV, and that is also the case in the narrow region where the 37 GHz brightness temperatures of both CRTM and RTTOV dip below 175 K. This may seem a priori surprising, because (7) is a conditional mean, and it should therefore not produce values that are greater than the maximum value in the database (and neither should it produce values that are smaller than the minimum value). This observation is correct, but it applies only to the quantity whose mean is being sought, namely, the transformed observations $\vec{a}_i^t \vec{O}'$, $i = 1, \ldots, m$. Because we are only using (7) with the first $m = 3$ maximum-correlation transforms in this example, and we are reconstituting the full vector of brightness temperatures $\vec{O}$ using archival means for the remaining six lower principal components, we cannot expect our approach to produce brightness temperature estimates that are exactly bounded by those in the database—and nor is that required in the assimilation, since we intend to

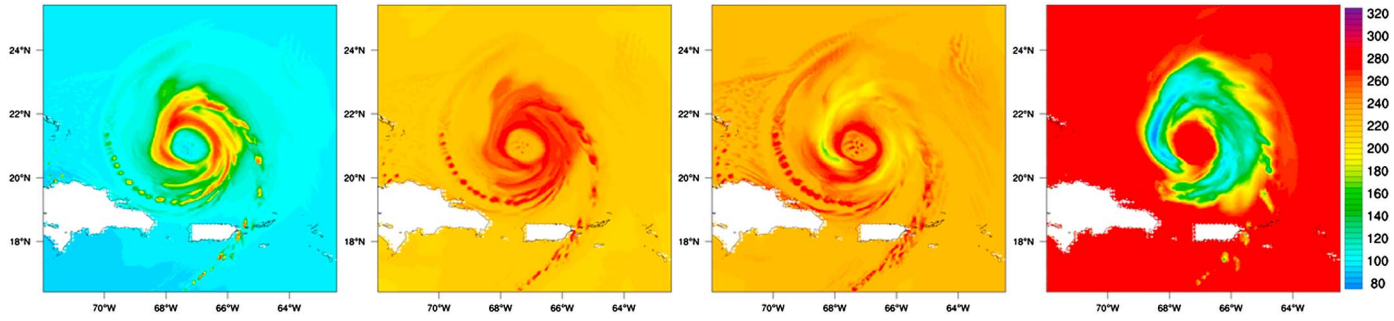

Figure 14. Brightness temperatures at the 10.7 GHz-Hpol, 19.3 GHz-Vpol, 37 GHz-Vpol, and 85.5 GHz-Vpol channels of TMI, calculated using RTTOV from the output of our HWRF simulation of Hurricane Earl at 0430 Z on 31 August 2010 (as in Figures 12 and 13).

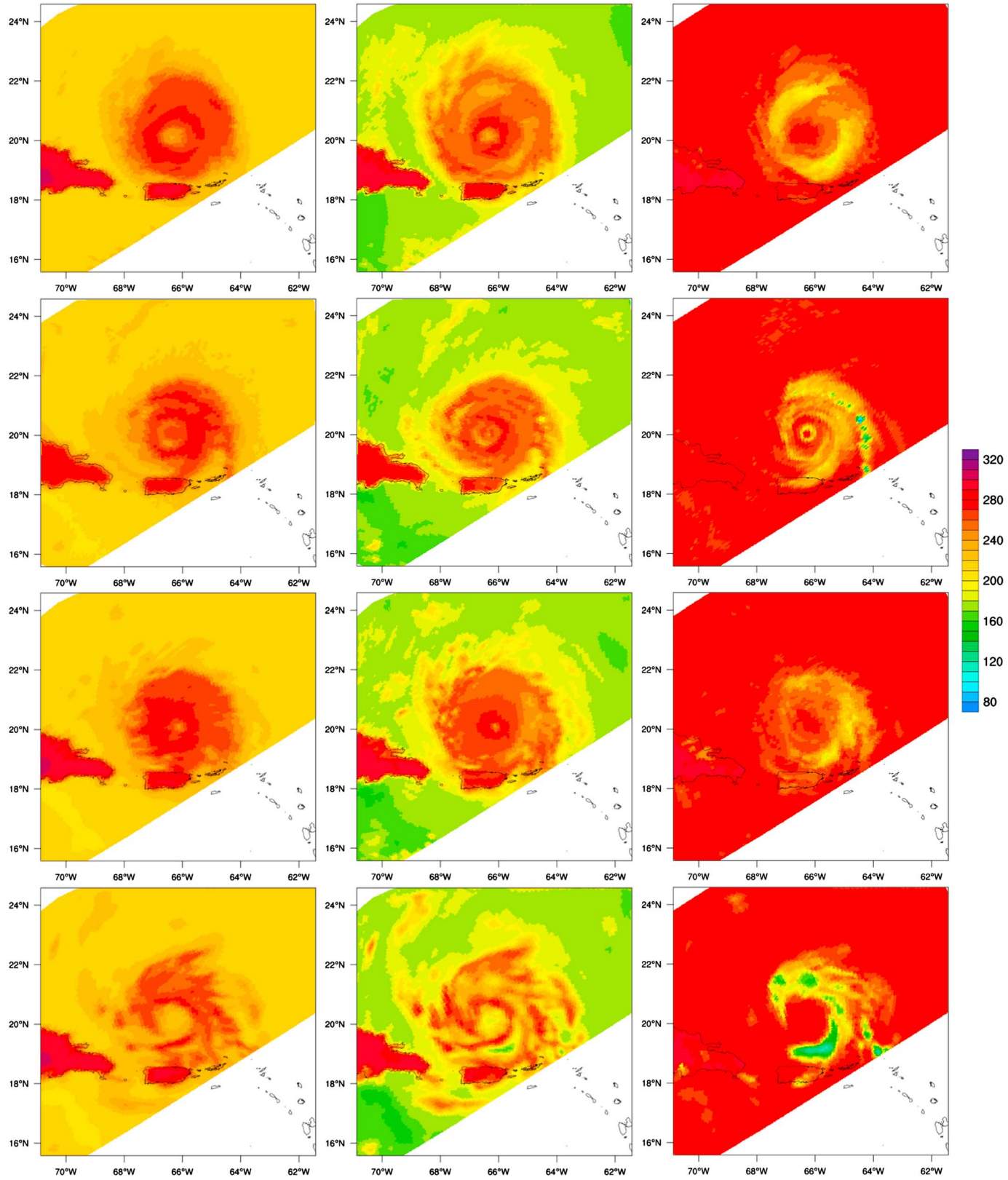

Figure 15. (first row) Brightness temperatures calculated using our operator for the ensemble mean of our HEDAS forecast of Hurricane Earl for 0430 Z on 31 August 2010, at the 19.3 GHZ-Vpol, 37 GHz-Hpol, and 85.5 GHz-Vpol channels of TMI. (second row) Actual TMI observations at 0439 Z. (third row) Brightness temperatures calculated using our operator for the analyzed variables at 0430 Z (postassimilation). (fourth row) Brightness temperatures calculated for the ensemble forecast at 0530 Z starting with the analysis at 0430 Z.

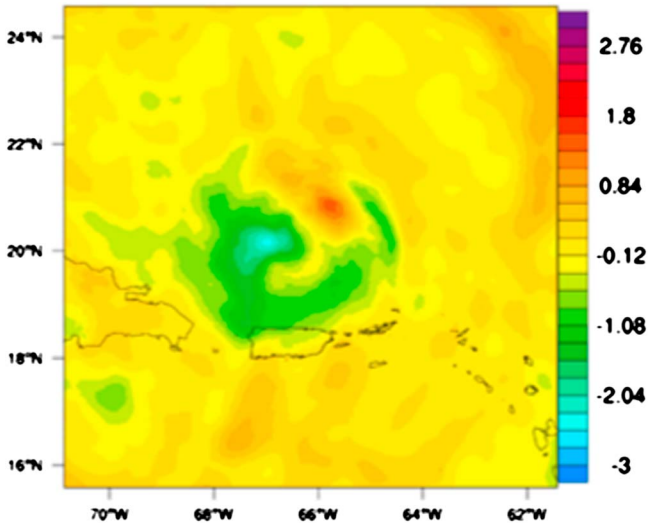

Figure 16. Pressure innovation in hectopascals for our ensemble data assimilation as in Figure 15.

assimilate the top maximum-correlation transform observations only, not the observed brightness temperatures themselves. One alternative would be to use (7) with $m = M$, i.e., to compute

$$\tau_j(\vec{x}, \vec{p}_b, \vec{p}_s) \;=\; C^{-1} \sum_{\vec{x}^{(k)} \in \text{database}} O_j^{(k)} \exp\left(-0.5 \sum_{j=1}^{m} \left[\vec{b}_j^t \vec{x}' - \vec{b}_j^t \vec{x}'^{(k)} \right]^2 \right) \tag{8}$$

where O_j is the brightness temperature in the jth TMI channel. In this alternative approach, (8) would be computed for each $j = 1, \ldots, M$, but one would then assimilate only the top maximum-correlation vectors $\vec{a}_i^t \vec{\tau}$ for $i = 1, 2, 3$ only. This alternative is likely to introduce errors due to the inability of the forward model—-and of the observations—to resolve the level of detail corresponding to the lower principal components. We are currently evaluating this alternative.

Figure 15 shows the evolution of the brightness temperatures through the ensemble data assimilation. Figure 15 (first row) illustrates the signatures for our ensemble mean background, Figure 15 (second row) shows the actual TMI measurements, Figure 15 (third row) shows the signatures of the analyzed field at the end of the TMI assimilation using our observation operator, and Figure 15 (fourth row) shows the signatures of the forecast 1 h after the TMI assimilation. Contrast the angular symmetry of the ensemble mean signatures with the pronounced asymmetry of the TMI observations and note how the assimilation tried to make the fields similarly asymmetric (Figure 15, third row), with this asymmetry persisting in the signatures shown in Figure 15 (fourth row) and calculated with our observation representation from the forecast fields 1 h after the assimilation. Figure 16 shows the surface pressure innovation, illustrating how the assimilation shifted the hurricane center west-southwest; Figure 17 shows the vertically averaged condensed water mass mixing

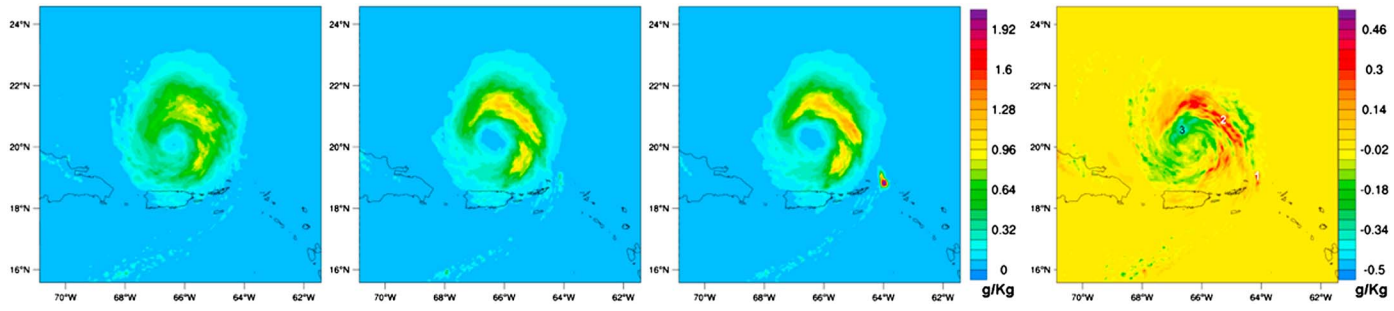

Figure 17. Vertically averaged condensed water mass mixing ratios, from the ensemble mean (first panel) before the assimilation and (second panel) after the assimilation, as well as (third panel) after a different assimilation where we divided the observation covariance matrix by 4 to increase the impact of the TMI observations. (fourth panel) The adjustment to the vertically averaged condensed water mass, with the three grid points selected for vertical examination highlighted.

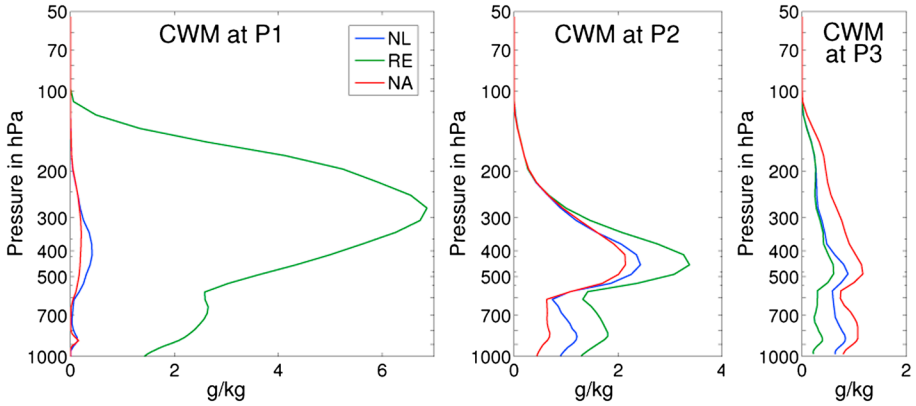

Figure 18. Vertical profiles of the condensed water mass at the three grid points highlighted in Figure 17 (fourth panel), with the background values (NA) in red, the analyzed values (NL) in blue, and the results of the assimilation with a fourfold reduction in the observation covariance (RE) in green.

ratios, from the ensemble mean before the assimilation (first panel) and after the assimilation (second panel), as well as after a different assimilation where we divided the observation covariance matrix by 4 to increase the impact of the TMI observations—note the more substantial increase in the condensed water mass, as well as the appearance of a convective area to the southeast. Finally, we chose three areas to illustrate the vertical distribution of the condensation before and after the assimilation: one in that area of convection that appeared when we reduced the observation covariance by a factor of 4, another in the rain band where the assimilation produced a more moderate increase in the condensed water mass, and one closer to the center of the system where the assimilation reduced the condensed water mass. Figure 18 shows the profiles in those three areas, the background values as well as the analyzed values for the two settings of the observation covariance. Note how our use of vertical principal components allows the assimilation to effect substantial changes in the condensed water profiles, with augmentations as well as reductions in the condensed mass as required by the optimization.

5. Conclusions

The approach described in this paper was developed to allow the efficient representation of the observation operator in the case of microwave observations of precipitation that accounts for the nonlinear effect of the variability of the model variables and the radiative parameters on the resulting microwave signatures. The approach produces a smooth function whose value can be very efficiently computed in real time, *along with all partial derivatives with respect to the control variables*, relying on a precompiled database that is meant to represent the range of plausible joint values of the variables and the parameters. The approach is illustrated by the specific case of "window-channel" passive microwave observations over a hurricane, but the method is applicable in a more general context, to represent nonlinear functions of a large number of random variables whose a priori means and covariances are given as empirical samples from realistic simulations. Indeed, the approach applies to simultaneous observations from different instruments (such as a radar and/or a microwave window-channel radiometer and/or a sounder, for example)—the dimensionality reduction step in the approach is general enough to apply to these scenarios to represent the first two moments of the resulting observation, i.e., the observation operator and the associated observation covariances. The resulting observation operator is much faster to run computationally than a forward radiative transfer model, but that is not its main attraction. Rather, it is the fact that it effectively accounts for the uncertainty in the variables and in the microphysical and radiative parameters, including the possibility of allowing for several microphysical assumptions, as would be required when the background does not come from a known scheme.

Acknowledgments
This work was performed at the Jet Propulsion Laboratory, California Institute of Technology, under contract with the National Aeronautics and Space Administration. The research was supported by a grant from the National Oceanic and Atmospheric Administration through the Hurricane Forecasting Improvement Project. The TRMM data and our forward simulations can be found at http://trmm.jpl.nasa.gov/2015JD023107_data/.

References

Aksoy, A., S. Lorosolo, T. Vukicevic, K. J. Sellwood, S. D. Aberson, and F. Q. Zhang (2012), The HWRF Hurricane Ensemble Data Assimilation System (HEDAS) for high-resolution data: The impact of airborne doppler radar observations in an OSSE, *Mon. Weather Rev.*, *140*, 1843–1862.

Aonashi, K., and H. Eito (2011), Displaced ensemble variational assimilation method to incorporate microwave imager brightness temperatures into a cloud-resolving model, *J. Meteorol. Soc. Jpn.*, *89*, 175–194.

Bauer, P., P. Lopez, A. Benedetti, D. Salmond, and E. Moreau (2006), Implementation of 1D+4D-Var assimilation of precipitation-affected microwave radiances at ECMWF: I. 1DVar, *Q. J. R. Meteorol. Soc.*, *132*, 2277–2306.

Boukabara, S.-A., et al. (2011), MiRS: An all-weather 1Dvar satellite data assimilation and retrieval system, *IEEE Trans. Geosci. Remote Sens.*, *49*, 3249–3272.

Chen, S.-H. (2007), The impact of assimilating SSM/I and QuikSCAT satellite winds on Hurricane Isidore simulations, *Mon. Weather Rev.*, *135*, 549–566.

Coppens, D., Z. S. Haddad, and E. Im (2000), Estimating the uncertainty in passive-microwave rain retrievals, *J. Atmos. Oceanic Technol.*, *17*, 1618–1629.

Errico, R. K., J.-F. Mahfouf, and P. Bauer (2007), Issues regarding the assimilation of cloud and precipitation data, *J. Atmos. Sci.*, *64*, 3785–3798.

Gopalakrishnan, S. G., F. Marks Jr., J. A. Zhang, X. Zhang, J.-W. Bao, and V. Tallapragada (2013), Study of the impacts of vertical diffusion on the structure and intensity of the tropical cyclones using the high-resolution HWRF system, *J. Atmos. Sci.*, *70*, 524–541.

Haddad, Z. S., J. P. Meagher, S. L. Durden, E. A. Smith, and E. Im (2007), Drop size ambiguities in the retrieval of precipitation profiles from dual-frequency radar measurements, *J. Atmos. Sci.*, *63*, 204–217.

Han, Y., P. van Delst, Q. Liu, F. Weng, B. Yan, R. Treadon, and J. Derber (2006), JCSDA Community Radiative Transfer Model (CRTM)—Version 1, *NOAA Tech. Report*, 122, NOAA, Washington, D. C.

Heidinger, A. K., C. O'Dell, R. Bennartz, and T. Greenwald (2006), The successive-order-of-interaction radiative transfer model: Part I. Model development, *J. Appl. Meteorol. Clim.*, *45*, 1388–1402.

Hong, S. Y., and J.-O. Lim (2006), The WRF single-moment 6-class microphysics scheme (WSM6), *J. Korean Meteorol. Soc.*, *42*, 129–151.

Hotelling, H. (1936), Relations between two sets of variates, *Biometrika*, *28*, 321–377.

Kummerow, C., W. Barnes, T. Kozu, J. Shiue, and J. Simpson (1998), The Tropical Rainfall Measuring Mission (TRMM) sensor package, *J. Atmos. Oceanic Technol.*, *15*, 809–817.

Matricardi, M., F. Chevalier, and S. Tjemkes (2001), An improved general fast radiative transfer model for the assimilation of radiance observations, *ECMWF Res. Dept. Tech. Memo.*, 345, ECMWF, Reading, U. K.

Michalakes, J., S. Chen, J. Dudhia, L. Hart, J. Klemp, J. Middlecoff, and W. Skamarock (2001), Development of a next-generation regional weather research and forecast model, in *Developments in Teracomputing: Proceedings of the Ninth ECMWF Workshop on the Use of High-Performance Computing in Meteorology*, edited by W. Zwieflhofer and N. Kreitz, pp. 269–276, World Scientific, Singapore.

Thompson, G., P. R. Field, R. M. Rasmussen, and W. D. Hall (2008), Explicit Forecasts of winter precipitation using an improved bulk microphysics scheme: Part II. Implementation of a new snow parameterization, *Mon. Weather Rev.*, *136*, 5095–5115.

Vukicevic, T., M. Sengupta, A. S. Jones, and T. Vonder Haar (2007), Cloud-resolving satellite data assimilation: Information content of IR window observations and uncertainties in estimation, *J. Atmos. Sci.*, *63*, 901–919.

Zhang, S. Q., M. Zupanski, A. Y. Hou, X. Lin, and S. H. Cheung (2012), Assimilation of precipitation-affected radiances in a cloud-resolving WRF ensemble data assimilation system, *Mon. Weather Rev.*, *141*, 754–772.